IOP Conference Series: Materials Science and Engineering

PAPER • OPEN ACCESS

Structure and mechanical properties of near-eutectic refractory Al-Cr-Nb-Ti-Zr high entropy alloys

To cite this article: N Yurchenko *et al* 2021 *IOP Conf. Ser.: Mater. Sci. Eng.* **1014** 012058

Structure and mechanical properties of near-eutectic refractory Al-Cr-Nb-Ti-Zr high entropy alloys

N Yurchenko*, E Panina, G Salishchev and N Stepanov

Laboratory of Bulk Nanostructured Materials, Belgorod National Research University, Belgorod 308015, Russia

*Corresponding author: yurchenko_nikita@bsu.edu.ru

Abstract. In this study, the structure and mechanical properties of the near-eutectic refractory $Al_{24}Cr_{11}Nb_{11}Ti_{37}Zr_{17}$, $Al_{20}Cr_{20}Nb_{25}Ti_{25}Zr_{10}$, and $Al_{28}Cr_{15}Nb_{15}Ti_{20}Zr_{22}$ (at.%) high entropy alloys were investigated. Both the $Al_{24}Cr_{11}Nb_{11}Ti_{37}Zr_{17}$ and $Al_{20}Cr_{20}Nb_{25}Ti_{25}Zr_{10}$ alloys had a hypoeutectic structure, while the $Al_{28}Cr_{15}Nb_{15}Ti_{20}Zr_{22}$ alloy had a hypereutectic one. The proeutectic phase in the $Al_{24}Cr_{11}Nb_{11}Ti_{37}Zr_{17}$ and $Al_{20}Cr_{20}Nb_{25}Ti_{25}Zr_{10}$ alloys was the ordered B2 phase and in the $Al_{28}Cr_{15}Nb_{15}Ti_{20}Zr_{22}$ alloy – the C14 Laves phase. In all three alloys, the eutectic regions possessed a fine lamellar structure composed of a mixture of the C14 Laves and B2 phases. The densities of the alloys were 5.20-5.89 g/cm^3. The $Al_{24}Cr_{11}Nb_{11}Ti_{37}Zr_{17}$ and $Al_{28}Cr_{15}Nb_{15}Ti_{20}Zr_{22}$ alloys were extremely brittle at 22°C, while the $Al_{20}Cr_{20}Nb_{25}Ti_{25}Zr_{10}$ alloy showed some ductility (ε = 0.7%) and high yield strength of 1830 MPa. At 800°C, all alloys became ductile. The highest yield strength (1010 MPa) was demonstrated by the $Al_{20}Cr_{20}Nb_{25}Ti_{25}Zr_{10}$ alloy and the lowest one (235 MPa) – by the $Al_{24}Cr_{11}Nb_{11}Ti_{37}Zr_{17}$ alloy. The comparison between the experimental as-solidified structures and the CALPHAD predictions was made.

1. Introduction

Refractory high entropy alloys (RHEAs) demonstrate exceptional resistance to softening at temperatures up to 1600°C that makes them attractive candidates for high-temperature applications [1]. RHEAs are usually based on single-phase bcc or ordered B2 solid solution and can also contain intermetallic secondary phases. However, the selection of a proper type of structure for the best mechanical properties is a complex task due to the variety of alloys' compositions.

Recent studies showed an intriguing option for the development of the RHEAs with a ductile bcc matrix and embedded coherent B2 nanoparticles that resembled the γ/γ' structure of commercial nickel-based superalloys [2]. Such a microstructure design enhances room-temperature plasticity but does not prevent the rapid strength loss at T > 600°C due to undesired phase transformations [3].

Higher performance at elevated temperatures can be achieved in RHEAs with a composite-like structure [4]. One of the notable examples of RHEAs composites is the $Al_{20}Cr_{10}Nb_{15}Ti_{20}V_{25}Zr_{10}$ alloy [5]. Owing to a hypoeutectic structure comprised of relatively soft B2 and hard C14 Laves phases, and low density (5.55 g/cm^3), the alloy was found to be one of the strongest RHEAs at 800°C. Unfortunately, the presence of V, which is harmful to oxidation resistance [6], can limit potential structural applications of this RHEA. In the current study, we reported several V-free variants of the $Al_{20}Cr_{10}Nb_{15}Ti_{20}V_{25}Zr_{10}$ alloy and investigated their structure and mechanical properties.

2. Materials and methods

The program alloys with nominal compositions of $Al_{24}Cr_{11}Nb_{11}Ti_{37}Zr_{17}$, $Al_{20}Cr_{20}Nb_{25}Ti_{25}Zr_{10}$, and $Al_{28}Cr_{15}Nb_{15}Ti_{20}Zr_{22}$ (at.%) were produced by vacuum arc melting. The phase composition and microstructure of the alloys were studied for the as-cast state using X-ray diffraction (XRD) and scanning electron microscopy (SEM). The densities of the $Al_{24}Cr_{11}Nb_{11}Ti_{37}Zr_{17}$, $Al_{20}Cr_{20}Nb_{25}Ti_{25}Zr_{10}$, and $Al_{28}Cr_{15}Nb_{15}Ti_{20}Zr_{22}$ alloys, determined by the hydrostatic weighing method, were 5.20 ± 0.02, 5.89 ± 0.03, and 5.50 ± 0.03 g/cm^3, respectively. Isothermal compression of rectangular samples measured 6×4×4 mm^3 was carried out at 22 °C or 800 °C. The initial strain rate was 10^{-4} s^{-1}. Sheil solidification diagrams were constructed using a Thermo-Calc (version 2020a) software and a TCHEA3 (high-entropy alloys) database.

3. Results and discussion

According to XRD analysis (Figure 1a), all program alloys had a dual-phase structure composed of B2 and C14 (hcp) Laves phases. The EBSD phase maps had shown that the $Al_{24}Cr_{11}Nb_{11}Ti_{37}Zr_{17}$ alloy had a hypoeutectic microstructure consisted of a proeutectic B2 (red color) phase separated by eutectic regions composed of the lamellar C14 Laves (green color) and B2 phases (Figure 1b). The $Al_{20}Cr_{20}Nb_{25}Ti_{25}Zr_{10}$ alloy also possessed the hypoeutectic microstructure (Figure 1c), similar to the $Al_{24}Cr_{11}Nb_{11}Ti_{37}Zr_{17}$ alloy. The $Al_{28}Cr_{15}Nb_{15}Ti_{20}Zr_{22}$ alloy showed the hypereutectic microstructure comprised of the proeutectic C14 Laves phase surrounded by eutectic (C14 Laves+B2) domains. According to EDS analysis (Table 1), the B2 phase, in all program alloys, was enriched with Ti and Nb, while the C14 Laves phase was enriched with Cr, Zr, and (slightly) Al.

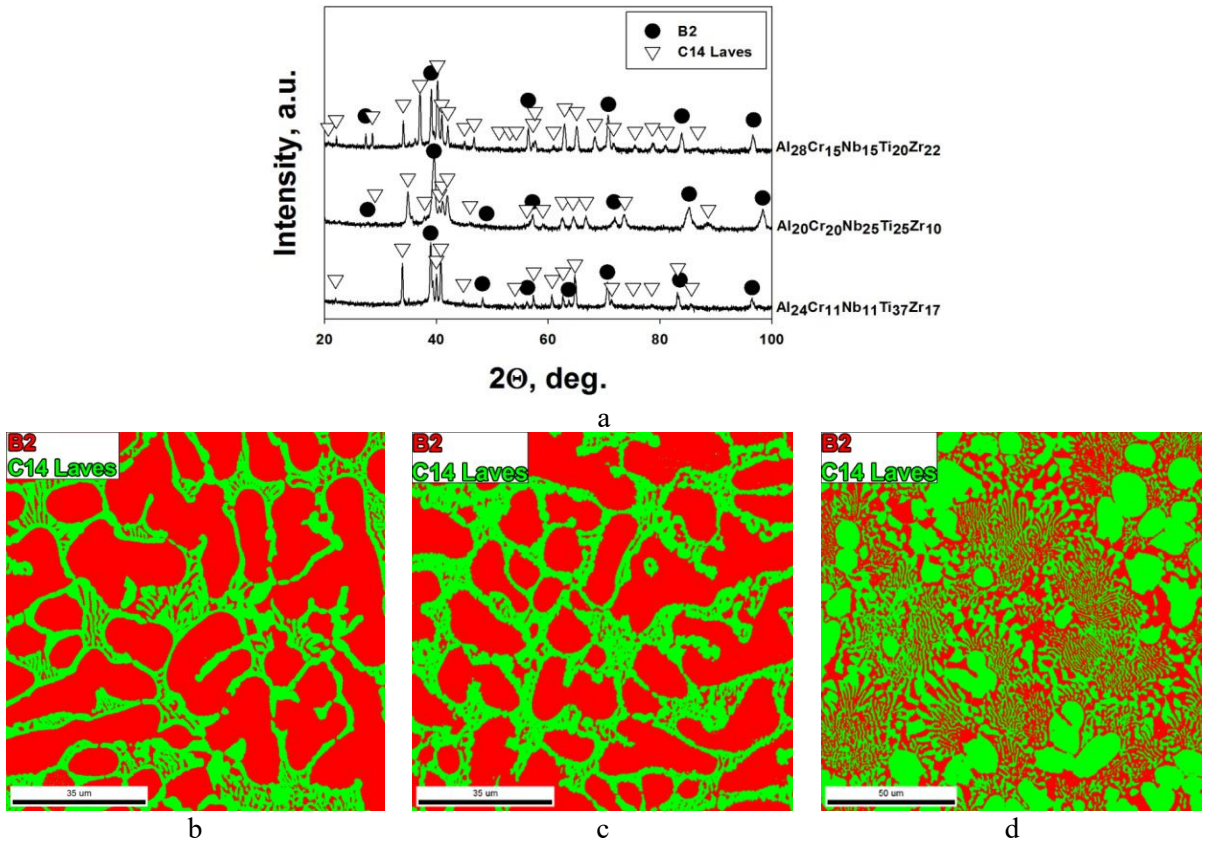

Figure 1. Structure of the $Al_{24}Cr_{11}Nb_{11}Ti_{37}Zr_{17}$ (a, b), $Al_{20}Cr_{20}Nb_{25}Ti_{25}Zr_{10}$ (a, c), and $Al_{28}Cr_{15}Nb_{15}Ti_{20}Zr_{22}$ (a, d) alloys; XRD pattern – a; EBSD phase maps – b-d.

Table 1. Chemical compositions of structural constituents of the $Al_{24}Cr_{11}Nb_{11}Ti_{37}Zr_{17}$, $Al_{20}Cr_{20}Nb_{25}Ti_{25}Zr_{10}$, and $Al_{28}Cr_{15}Nb_{15}Ti_{20}Zr_{22}$ alloys.

Element, at.%	Al	Cr	Nb	Ti	Zr	Volume fraction, %
$Al_{24}Cr_{11}Nb_{11}Ti_{37}Zr_{17}$						
B2 phase	22.2	8.2	14.0	41.4	14.2	69±2
C14 Laves phase	25.2	14.7	9.1	28.7	22.3	31±2
Alloy composition	23.7	10.7	11.9	36.2	17.5	-
$Al_{20}Cr_{20}Nb_{25}Ti_{25}Zr_{10}$						
B2 phase	19.5	14.9	30.2	29.5	5.9	64±1
C14 Laves phase	22.3	27.8	16.8	17.8	15.3	36±1
Alloy composition	20.8	20.0	25.1	25.2	8.9	-
$Al_{28}Cr_{15}Nb_{15}Ti_{20}Zr_{22}$						
C14 Laves phase	30.3	20.8	11.5	11.4	26.0	58±2
B2 phase	23.8	6.9	20.8	31.3	17.2	42±2
Alloy composition	27.5	14.6	15.8	19.8	22.3	-

Figure 2 presents the engineering stress-strain curves of the $Al_{24}Cr_{11}Nb_{11}Ti_{37}Zr_{17}$, $Al_{20}Cr_{20}Nb_{25}Ti_{25}Zr_{10}$, and $Al_{28}Cr_{15}Nb_{15}Ti_{20}Zr_{22}$ alloys obtained during compression at 22 and 800 °C. At 22°C, the $Al_{24}Cr_{11}Nb_{11}Ti_{37}Zr_{17}$ and $Al_{28}Cr_{15}Nb_{15}Ti_{20}Zr_{22}$ alloys fractured in the elastic region at 1570 and 795 MPa, respectively (Figure 2a). In turn, the $Al_{20}Cr_{20}Nb_{25}Ti_{25}Zr_{10}$ alloy showed some ductility (ε = 0.7%) and a high yield strength of 1830 MPa. At 800 °C, the program alloys became ductile (Figure 2b). The $Al_{24}Cr_{11}Nb_{11}Ti_{37}Zr_{17}$ alloy had the lowest yield strength of 285 MPa and, after attaining the yield point, showed a prolonged steady-state flow stage. In the $Al_{28}Cr_{15}Nb_{15}Ti_{20}Zr_{22}$ alloy, after yielding at 685 MPa, a notable strengthening stage followed by softening, and then a steady-state flow stage was observed. The $Al_{20}Cr_{20}Nb_{25}Ti_{25}Zr_{10}$ alloy was the strongest with a yield strength of 1010 MPa. Despite the impressive work hardening capacity resulting in a peak stress value of 1225 MPa, the alloy then gradually softened until reaching ~26-27% of plastic deformation; flow stress stabilized at a level of ~780-800 MPa.

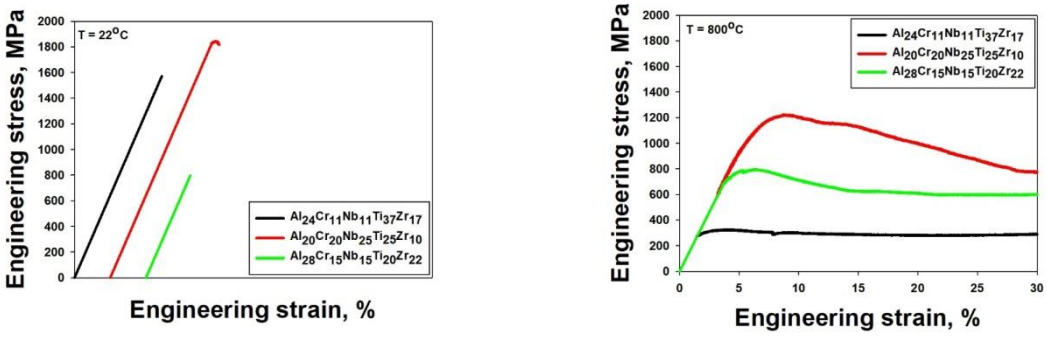

a b

Figure 2. Engineering stress-strain curves of the program alloys obtained during compression at 22 °C (a) and 800 °C (b).

The CALPHAD method was used to analyze the experimental structures of the program alloys (Figure 3). According to the Scheil solidification diagrams, crystallization of all three alloys should start at ~1700 °C, but terminate differently: at ~1450 °C ($Al_{24}Cr_{11}Nb_{11}Ti_{37}Zr_{17}$), ~1500 °C ($Al_{20}Cr_{20}Nb_{25}Ti_{25}Zr_{10}$), and 1350 °C ($Al_{28}Cr_{15}Nb_{15}Ti_{20}Zr_{22}$). The solidification of the $Al_{24}Cr_{11}Nb_{11}Ti_{37}Zr_{17}$ alloy is expected to follow the sequence of L→L+bcc→L+bcc+C14 Laves (Figure 3a). At the same time, in the $Al_{20}Cr_{20}Nb_{25}Ti_{25}Zr_{10}$ and $Al_{28}Cr_{15}Nb_{15}Ti_{20}Zr_{22}$ alloys, the sequence of L→L+C14 Laves→L+bcc+C14 Laves is predicted (Figures 3b, c). Note that the L+C14

Laves→L+bcc+C14 Laves transition in the $Al_{20}Cr_{20}Nb_{25}Ti_{25}Zr_{10}$ alloy should occur in a very narrow temperature interval, thereby suggesting a "eutectic-like" reaction of L→L+bcc+C14 Laves (Figure 3b).

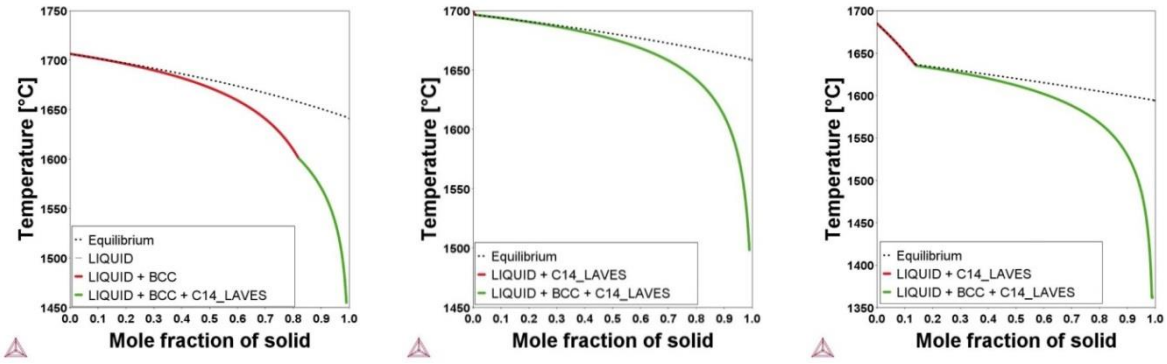

a b c

Figure 3. Scheil solidification diagrams of the $Al_{24}Cr_{11}Nb_{11}Ti_{37}Zr_{17}$ (a), $Al_{20}Cr_{20}Nb_{25}Ti_{25}Zr_{10}$ (b), and $Al_{28}Cr_{15}Nb_{15}Ti_{20}Zr_{22}$ (c) alloys.

To sum up, we introduced three new RHEAs with composite-like near-eutectic structures composed of B2 and C14 Laves phases and a rather low density of 5.20-5.89 g/cm^3. Two alloys, $Al_{24}Cr_{11}Nb_{11}Ti_{37}Zr_{17}$ and $Al_{20}Cr_{20}Nb_{25}Ti_{25}Zr_{10}$, had the hypoeutectic microstructure, meanwhile the $Al_{28}Cr_{15}Nb_{15}Ti_{20}Zr_{22}$ alloy – the hypereutectic one. Among the program alloys, the $Al_{20}Cr_{20}Nb_{25}Ti_{25}Zr_{10}$ showed the best combination of mechanical properties: modest ductility at 22 °C and the highest yield strength at 22 and 800 °C. It was found that CALPHAD correctly predicted the as-solidified microstructures of the $Al_{24}Cr_{11}Nb_{11}Ti_{37}Zr_{17}$ and $Al_{28}Cr_{15}Nb_{15}Ti_{20}Zr_{22}$ alloys, but failed in the case of the $Al_{20}Cr_{20}Nb_{25}Ti_{25}Zr_{10}$ alloy; the B2 ordering of the bcc phase was not anticipated in any of the alloys. Such inaccuracies must be taken into account during the design of novel (near)-eutectic RHEAs with advanced properties based on the Al-Cr-Nb-Ti-Zr alloy system.

Acknowledgments
The authors gratefully acknowledge the financial support from the Russian Science Foundation Grant no. 19-79-30066.

References

[1] Senkov O N, Miracle D B and Chaput K J 2018 Development and exploration of refractory high entropy alloys — A review *J. Mater. Res.*
[2] Soni V, Senkov O N, Gwalani B, Miracle D B and Banerjee R 2018 Microstructural Design for Improving Ductility of An Initially Brittle Refractory High Entropy Alloy *Sci. Rep.* 1–10
[3] Senkov O N, Couzinie J-P, Rao S I, Soni V and Banerjee R 2020 Temperature dependent deformation behavior and strengthening mechanisms in a low density refractory high entropy alloy Al10Nb15Ta5Ti30Zr40 *Materialia* 100627
[4] Liu Y, Zhang Y, Zhang H, Wang N, Chen X, Zhang H and Li Y 2017 Microstructure and mechanical properties of refractory HfMo0.5NbTiV0.5Six high-entropy composites *J. Alloys Compd.* **694** 869–76
[5] Yurchenko N, Panina E, Tikhonovsky M, Salishchev G, Zherebtsov S and Stepanov N 2020 Structure and mechanical properties of an in-situ refractory Al20Cr10Nb15Ti20V25Zr10 high entropy alloy composite *Mater. Lett.* 127372
[6] Butler T M, Chaput K J, Dietrich J R and Senkov O N 2017 High temperature oxidation behaviors of equimolar NbTiZrV and NbTiZrCr refractory complex concentrated alloys (RCCAs) *J. Alloys Compd.* **729** 1004–19